MEASUREMENTS AND MODELING OF SOOT AND CO POLLUTANT EMISSIONS IN A LARGE OIL FIRED FURNACE

Mohammad Moghiman*

Faculty of Engineering, Ferdowsi University of Mashhad, Iran

Ali Saeedi

Islamic Azad University of Gonabad, Iran

Mohammad Javadi and Vahid Etminan

Faculty of Engineering, Ferdowsi University of Mashhad, Iran

الخلاصة:

يقدم هذا البحث ويحلل إنتاج السخام الملوث وانبعاثه مع الغاز أول أكسيد الكربون بوساطة فرن أسطواني الشكل بطول قابل للتغيير وبطاقة اثنين ميجاوات. وقد تمت عملية قياسات التجارب عن طريق تقنية الأشعة تحت الحمراء وورق الترشيح لقياس كل من غاز أول أكسيد الكربون والسخام على التوالي. وتم تمثيل تكوين السخام عن طريق عد كثافة الجسيمات والكثافة الكتلية المبنية على تركيز الاستلين. كما تم تمثيل أكسدة السخام بوساطة أنموذج أكسدة الأكسجين مع الهيدروكسيل $O_2 - OH$. الذي يفترض أن احتراق السخام يتم عن طريق كل من جزيئات الأكسجين ومجموعة الهيدروكسيل. وقد تطابقت نتائج البحث المعملية من حيث تفاوت الحرارة وغاز أول أكسيد الكربون والسخام عند أربعة مقاطع عرضية محورية ، وكذلك تطابق تأثير طول الفرن على إنبعاث الملوثات مع ماهو متوقع من نتائج. وأكدت الدراسة على نقصان جزء الكتلة لكل من غاز أول أكسيد الكربون والسخام مع زيادة طول الفرن. كما أكدت على أن موقع المركز لقمة السخام يتطابق وموقع قمة غاز أول أكسيد الكربون.

* Corresponding author:

E-mail: mmoghiman@yahoo.com

Paper Received May 13, 2008; Paper Revised May 11, 2009; Paper Accepted May 27, 2009

ABSTRACT

This paper presents and analyses the production and emission of pollutant soot and CO from a 2 MW cylindrical furnace of variable length. The experimental measurements were carried out using infra-red and filter paper techniques to measure CO and soot, respectively. The soot formation is modeled by using the soot particle number density and the mass density based on acetylene concentrations. The soot oxidation is modeled using the $O_2 - OH$ oxidation model, which assumes soot combustion occurs by both oxygen molecules and hydroxide radicals. The predicted radial variations of temperature, CO, and soot at four axial cross sections, and the effect of furnace length on pollutant emissions, compare well with the experimental measurements. The results show that CO and soot mass fraction emissions decrease with increasing furnace length. The results also show that the location of the centerline soot maximum coincides with the maximum CO location.

***Key words*:** soot formation/combustion, large oil-fired furnace, filter paper technique, spray combustion

MEASUREMENTS AND MODELING OF SOOT AND CO POLLUTANT EMISSIONS IN A LARGE OIL FIRED FURNACE

1. INTRODUCTION

Industrial furnaces have wide applications in engineering, such as the extraction of metal from ore, or in oil refineries and other chemical plants [1]. In power plants, furnaces play a crucial role in transferring chemical energy stored in fossil fuels into heat. Much of this high-temperature equipment utilizes large amounts of liquid fuel and emits many pollutants such as soot and carbon monoxide (CO). The carbon monoxide chemistry is a very important part of the combustion of any carbohydrate, since nearly all carbon atoms are first oxidized to carbon monoxide, and only then to carbon dioxide. Wide-ranging concerns for the environmental impact of exhaust emissions from spray combustion, including oil fired furnaces, has recently added fresh impetus to research into the mechanisms of soot formation in flames and smoke production in practical combustion systems [2,3]. The detailed process of soot production from hydrocarbon fuels consists of complex chemical and physical steps, including fuel pyrolysis, formation of polycyclic aromatic hydrocarbons, particle inception, coagulation, surface growth, and combustion [4]. Kinetic studies reveal a dominant kinetic pattern of aromatic-ring growth, H-abstraction, and C_2H_2 addition [5]. The successful modeling of soot yield depends on both soot formation and oxidation models. The soot formation models, based on the assumption that soot inception and surface growth is a function of acetylene concentration, have been successfully used by many investigators [6]. In soot oxidation, the *OH* radical and molecular oxygen O_2 are the most important species, because, as oxygen is consumed rapidly in the vicinity of the inlet port, the *OH*-radical is an important oxidant along with the combustor [7,8].

The aim of the present work is the measurement and prediction of soot and CO emissions from turbulent spray flames in a 2 MW furnace and the investigation of the effects of furnace length and C/O ratio on soot and CO production. The computations are conducted considering fuel penetration, evaporation, combustion, and soot and CO formation under different operating conditions.

2. TEMPERATURE POLLUTANTS CONCENTRATION MEASUREMENT

The tests have been carried out on a large-scale cylindrical furnace identical to that reported previously [9]. The length of the furnace is relatively long (4300 mm) and is 800 mm in diameter (Fig. 1). The furnace is constructed with five movable sections (each 600 mm long). The total length of the furnace can be adjusted by adding or removing any of these sections. The inner surface of the furnace is refractory lined by a 22 mm thick layer. As shown in Figure 1, six sampling and measurement ports are positioned downstream from the burner nozzle at 0.3, 0.9, 1.5, 2.1, 2.7, and 4.25 m axial distance from the burner. These ports allow continuous access along the furnace length, which permits the introduction of measuring probes for in-flame measurement at any location. The temperature of gases is kept at 280 $^{\circ}$C in their path to avoid condensation of sample gases.

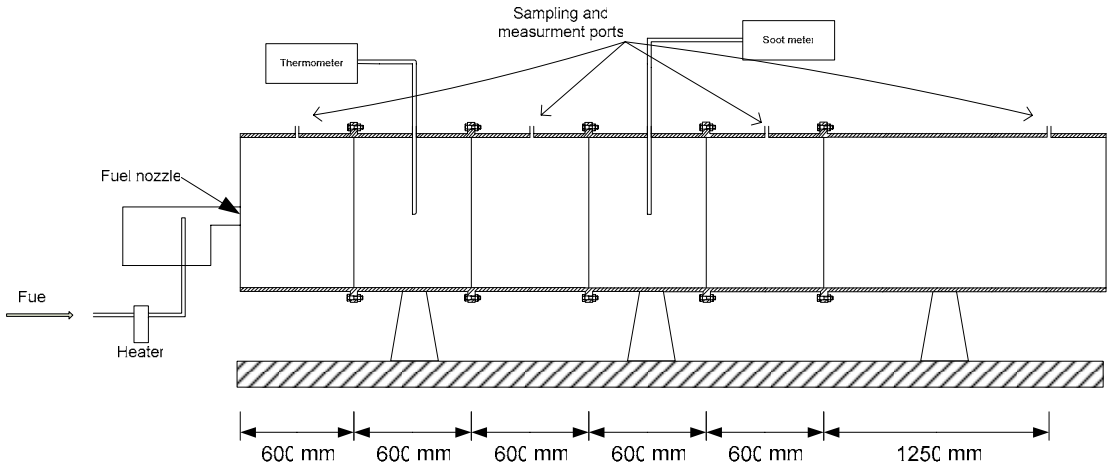

Figure 1. Schematic of oil fired furnace

The oil burner is a pressure jet oil burner with a 2.2 MW maximum power rating. The fuel is supplied to the nozzle at a pressure of 2.5 Mpa. The fuel and air flow rate are adjustable using the oil pump and the burner air valve, respectively. A variable swirl burner provides near-burner zone high mixing rates of air and fuel. Fuel is heated up by an electrical heater and then it is injected to the furnace through a 60 ° hollow-cone nozzle. Gas-oil is the sample fuel used throughout this study. The fuel has a viscosity of 1.5 to 5.5 cSt at 40 °C. Other properties of the fuel are as follows: initial density: $\rho_0=8.3\times10^2$ kgm^{-3}, vaporization temperature: $T_{vap}=373$ K, boiling point: $T_{boil}=462$ K, latent heat of vaporization: $\Delta H_{vap}=3.6\times10^5$ Jkg^{-1}, specific heat: $c_p=2.005\times10^3$ Jkg^{-1}K^{-1}, percent nitrogen in weight: 0.09.

A K-Type thermocouple, which withstands high temperatures, is used to provide temperature measurements within the furnace. The thermocouple is directly coupled with a voltmeter which shows the temperature in celsius. The described system measured temperatures within a tolerance of 1 °C .The stainless steel water-cooled probe (6 mm-id) provides samples for continuous, online gas analysis. Soot concentration is measured using the filter paper technique within a tolerance of 5e-8 soot volume fraction (AVL LIST GMBH 2001) [10]. This technique is an optical method whose results are dependent on the soot reflective index. The soot concentration value can be display as required in FSN (which used to be known as the Bosch filter smoke number), in mg/m^3 , or in % pollution level. The FSN is calculated from the paper blackening and effective length with the aid of table which describe the relation between filter load (mg soot/ m3) and paper blackening [10]. Even extremely low soot concentration in the exhaust gas can be measured because the sample volume can be varied. The uncertainty associated with the soot volume fraction measurements was dominated by uncertainty of the temperature measurements. The overall uncertainty in the temperature measurements was estimated to be 4%. The uncertainty of the soot volume fraction measurements is estimated to be 10 to 20%. The CO concentration was measured by an infrared IR100 Series Gas Analyzer. The IR100 is a non-dispersive, single-beam infrared gas analyzer that measures CO and other species, including CO_2 and CH_4.

3. THEORETICAL FORMULATION

The mathematical model was based on a typical Eulerian gas phase and a Lagrangian droplet phase formulation. Since a one-way interaction model was used for the gas flow and the droplet trajectory analysis, the air flow field was first evaluated and the results were used for evaluation of the droplet trajectories.

Gas phase conservation equations:

The time averaged gas phase equations are as follows:

Continuity:

$$\frac{\partial u}{\partial x}+\frac{1}{r}\frac{\partial}{\partial r}(rv)=\dot{S} \tag{1}$$

Momentum:

$$\frac{1}{r}\left[\frac{\partial}{\partial x}(r\rho uu)+\frac{\partial}{\partial r}(r\rho uv)\right]=-\frac{\partial p}{\partial x}+\mu\nabla^2 u-\frac{1}{r}\frac{\partial}{\partial r}(r\rho\overline{u'v'})-\frac{\partial}{\partial x}(\rho\overline{u'u'}) \tag{2}$$

$$\frac{1}{r}\left[\frac{\partial}{\partial x}(r\rho uv)+\frac{\partial}{\partial r}(r\rho vv)-\rho w^2\right]=-\frac{\partial p}{\partial r}+\mu(\nabla^2 v+\frac{v}{r^2})-\frac{1}{r}\frac{\partial}{\partial r}(r\rho\overline{v'v'})-\frac{\partial}{\partial x}(\rho\overline{u'v'})-\frac{1}{r}\rho\overline{w'w'} \tag{3}$$

and

$$\frac{1}{r}\left[\frac{\partial}{\partial x}(r\rho uw)+\frac{\partial}{\partial r}(r\rho vw)+\rho vw\right]=\mu(\nabla^2 w-\frac{w}{r^2})-\frac{1}{r}\frac{\partial}{\partial r}(r\rho\overline{v'w'})-\frac{\partial}{\partial x}(\rho\overline{u'w'})-\frac{1}{r}\rho\overline{v'w'} \tag{4}$$

where source term is represented by $\dot{S}$ arising from the mass interaction between gas and droplets. In view of the inability of the $k-\varepsilon$ model to cope with anisotropic flows according to [11], the turbulent stresses are calculated from an algebraic stress model [12].

Energy:
$$\frac{1}{r}\left[\frac{\partial}{\partial x}(r\rho uh)+\frac{\partial}{\partial x}(r\rho vh)\right]=\Gamma_h\nabla^2 h-\frac{1}{r}\frac{\partial}{\partial r}(r\rho\overline{v'h'})-\frac{\partial}{\partial x}(\rho\overline{u'h'})+\dot{S}_h+\dot{S}_R \tag{5}$$

The energy source terms ($\dot{S}_h+\dot{S}_R$) are the energy generated due to chemical reaction and radiation. The radiation contribution to the enthalpy equation is evaluated by the four flux radiation model [2]. The effect of soot, which is usually the dominant radiating species in hydrocarbon-fueled flames, on the radiative heat transfer inside the combustor is calculated by using a modified absorption coefficient (a) of the gas as [13, 14]

$$a_m = a + b_1 \rho\, m_S \left[1 + b_T (T - 2000)\right] \tag{6}$$

where a_m is the modified absorption coefficient, a the absorption coefficient, b_1 the empirical coefficient, ρ the gas phase density, m_s the soot mass fraction, b_T the empirical coefficient, and T is the mean temperature.

Individual species conservation:

$$\frac{1}{r}\left[\frac{\partial}{\partial x}(r\rho u m_j) + \frac{\partial}{\partial r}(r\rho v m_j)\right] = \Gamma_{mj}\nabla^2 m_j - \frac{1}{r}\frac{\partial}{\partial r}(r\rho \overline{v' m_j'}) - \frac{\partial}{\partial x}(\rho \overline{u' m_j'}) + R_j + S_j \tag{7}$$

where R_j is the mass rate of reaction or depletion by gas-phase chemical reactions, S_j is the rate of creation by vaporization occurring on the surface of the individual droplets, and Γ_{mj} is the laminar exchange coefficient.

Liquid phase: Evaporation and combustion of liquid fuels play an important role in producing pollutants. It is assumed that the second phase consists of spherical particles (droplets) dispersed in the continuous phase and that their contact is considered negligible due to rapid evaporation. Equations of displacement and velocity gradient in the Lagrangian system for each group *i* of fuel particles are as follows [15,16]:

$$\frac{d\vec{X}_{di}}{dt} = \vec{U}_{di} \tag{8}$$

$$m\frac{d\vec{U}_{di}}{dt} = \frac{\pi}{8}D_d^2\rho_d C_D\left(\vec{U}_d - \vec{U}\right)\left|\vec{U}_d - \vec{U}\right| + m_i\vec{g}\,(\rho_d - \rho)/\rho_d + \vec{F} \tag{9}$$

where m is droplet mass, U the gas velocity, U_d the droplet velocity, D_d the droplet diameter, ρ_d the fuel density, g the gravitational acceleration, F the centrifugal force produced by vortex motion, and C_D is the drag force which is obtained using the following equations:

$$\begin{aligned} C_D &= \frac{24}{\mathrm{Re}}\left[1 + \mathrm{Re}^{2/3}/6\right]; \quad && \mathrm{Re} < 1000 \\ C_D &= 0.44 && \mathrm{Re} > 1000 \end{aligned} \tag{10}$$

As the droplet enters the combustion chamber, droplet temperature T_d increases because of radiation and convection heat transfer and is described as follows:

$$m_d c_p \frac{dT_d}{dt} = hA_d\left(T_\infty - T_d\right) + E_d A_d \sigma\left(\tau_R^4 - T_d^4\right) \tag{11}$$

where m_d is droplet mass (kg), c_p the specific heat of droplet (J/kg·K), A_d the droplet surface area (m^2), T_∞ the gas local temperature (K), h the convection heat transfer coefficient (W/m^2·K), E_d the droplet emission coefficient (dimensionless), σ the Boltzmann constant, and τ_R is radiation temperature ($\tau_R = (I/4\sigma)^{1/4}$) in which I is emission intensity (W/m^2). Ranz and Marshal have proposed an equation for calculating h [17] as

$$\mathrm{Nu} = \frac{hD_d}{k_\infty} = 2.0 + 0.6\,\mathrm{Re}^{1/2}\,\mathrm{Pr}^{1/3} \tag{12}$$

where D_d is droplet diameter (m), k_∞ the gas conductivity (W/m·K), Re the Reynolds number ($\mathrm{Re}=\rho D_d|u_d - U|/\mu$), and Pr is the Prandtl number for the gas phase ($c_p\mu/k_\infty$). Mass transfer between two phases begins as soon as the droplet reaches vaporization temperature. The fuel vaporization rate is a function of vapor concentration on the droplet surface and the fuel vapor concentration in gas phase around the droplet:

$$N_{fu} = k_c\left(\frac{P_{\mathrm{sat}}}{\mathrm{R}T_d} - X_{fu}\cdot\frac{P_{\mathrm{op}}}{\mathrm{R}T_\infty}\right) \tag{13}$$

in which N_{fu} is the vapor mole flux (mol/m^2·s), k_c the mass transfer coefficient (m/s), P_{sat} the fuel vapor saturation pressure in droplet temperature T_d, R the universal gas constant, X_{fu} the fuel mole fraction around the droplet, and P_{op} and T_∞ are gas pressure and temperature, respectively. The mass transfer equation is obtained from Equation 14:

$$K_c = \frac{\Gamma_{fu}}{D_d}\left(0.2 + 0.6\,\mathrm{Re}^{1/2}\,\mathrm{Sc}^{1/3}\right) \tag{14}$$

where Γ_{fu} is the fuel vapor diffusion coefficient in gas phase (m^2/s) and Sc is the Schmidt coefficient ($\mu D_d/\rho$). Vapor flux, which is calculated from Equation 13, is used as a part of a source term in the fuel transport equation. The droplet mass is calculated as

$$m_d(t+\Delta t) = m_d(t) - N_{fu} A_d M_{fu} \Delta t \tag{15}$$

in which M_{fu} is fuel molecular weight. In this case, the droplet temperature is calculated from equations similar to Equation 11. The only difference is that the term $(dm/dt)h_{fg}$, in which h_{fg} is the fuel latent heat (J/kg), is added to the right side of Equation 11. Assuming that the droplet mass is not totally evaporated prior to reaching the boiling temperature (so the remaining mass reaches the fuel boiling temperature T_{db}), for constant droplet temperature, the boiling rate is obtained from Equation 16.

$$-\frac{dm_d}{dt} = hA\left(T_\infty - T_d\right) + A_d E_d \sigma\left(\tau_R^4 - T_d^4\right) \tag{16}$$

In addition, droplet diameter change is calculated as follows [18]:

$$-\frac{dD_d}{dt} = \frac{2}{\rho_d h_{fg}}\left[\frac{2k_\infty\left(1+0.23\sqrt{\mathrm{Re}_D}\right)}{D_d}\right]\left(T_\infty - T_d\right) + E_d\sigma\left(\tau_R^4 - T_d^4\right) \tag{17}$$

The energy required for evaporating the droplet is inserted with a negative sign in the source term of the energy equation for the gas phase.

Combustion: In this study, the effect of turbulence on the reaction rate is taken into account by employing the Eddy-Dissipation Concept (EDC) of Magnussen and Hjertager [19]. The chemical formula of gas oil is considered as $C_{15}H_{28}$ and the two-step process is used for modeling combustion.

Soot formation: The emission of soot from a flame is determined by a competition between soot formation and oxidation that must be considered when a soot modeling study is carrying out. In this study, a recent soot model developed by Moss [20] is used. The model describes the soot formation in terms of the soot particle number density (N) and the soot particle mass density (M) and takes into account the inception (nucleation), coagulation, growth, and oxidation processes for the rates of these two model parameters as

$$\frac{DN}{Dt} = \left(\frac{dN}{dt}\right)_{Inception} + \left(\frac{dN}{dt}\right)_{Coagulation} \tag{18}$$

and

$$\frac{DM}{Dt} = \left(\frac{dM}{dt}\right)_{Inception} + \left(\frac{dM}{dt}\right)_{Growth} + \left(\frac{dM}{dt}\right)_{Oxidation} \tag{19}$$

The acetylene inception model is used for the calculation of the soot inception rate according to Brookes and Moss [7], and Bashirnezhad *et al.* [21]. Taking into account that the presence of aromatics in liquid fuels enhances inception, the inception rates are computed by

$$\left(\frac{dN}{dt}\right)_{Inception} = c_1 N_A \left(\rho \frac{m_{C_2H_2}}{W_{C_2H_2}}\right) e^{-21100/T} \tag{20}$$

and

$$\left(\frac{dM}{dt}\right)_{Inception} = \frac{M_P}{N_A}\left(\frac{dN}{dt}\right)_{Inception} \tag{21}$$

where M_p , the mass of a soot nucleus, has a value of 144 kg $kmol^{-1}$ based on the assumption that the soot size corresponds to 12 carbon atoms and c_1 =54 s^{-1} is determined by [7].

Assuming the particles are monodispersed in size and spherical, the coagulation rate and reaction surface are given by:

$$\left(\frac{dN}{dt}\right)_{coagulation} = -\left(\frac{24R}{\rho_{Soot} N_A}\right)^{1/2}\left(\frac{6}{\pi\rho_{Soot}}\right)^{1/6} T^{1/2} M^{1/6} N^{11/6} \tag{22}$$

and

$$\left(\frac{dM}{dt}\right)_{growth} = c_2\left(\rho\frac{m_{C_2H_2}}{W_{C_2H_2}}\right)e^{-21100/T}\times\left((\pi N)^{1/3}\left(\frac{6M}{\rho_{Soot}}\right)^{2/3}\right) \tag{23}$$

where R is the universal gas constant, $\rho_{soot} = 2000 kgm^{-3}$, and c_2=9000.6 kg.m.kmol^{-1}.s^{-1} according to [22].

To predict soot oxidation, the O_2-OH oxidation is used. This model includes oxidation of soot as a result of an attack by both molecular oxygen O_2 and OH radicals. As oxygen is consumed rapidly in the vicinity of the inlet port, OH-radical is an important oxidant along the combustor. More direct measurements have indicated that OH is an important oxidant of soot, especially in the regions of diffusion flames where O_2 oxidation is minimal [8].

In this model, the rate of soot oxidation is given by

$$\left(\frac{dM}{dt}\right)_{Oxidation} = -c_4\rho\eta\frac{m_{OH}}{W_{OH}}\sqrt{T}(\pi N)^{1/3}\left(\frac{6M}{\rho_{Soot}}\right)^{2/3} - c_3\rho\frac{m_{O_2}}{W_{O_2}}\exp(\frac{-19778}{T})\sqrt{T}(\pi N)^{1/3}\left(\frac{6M}{\rho_{Soot}}\right)^{2/3} \tag{24}$$

where $\eta = 0.13$ and c_4=105.81 $kg.m.kmol^{-1}.K^{-1/2}$.s^{-1}, which are obtained by converting the rate of soot mass consumption [22] and c_3 = 8903.51 $kg.m.kmol^{-1}.K^{-1/2}$ [21].

4. NUMERICAL SOLUTION AND BOUNDARY CONDITIONS

An early version of Fluent, (Sprint code) has been developed and used for the simulations of processes inside the large oil-fired furnace [23]. The gas conservation equations are solved using a control-volume based computational procedure [24]. The convective terms are discretized by the power law scheme. The flow field pressure linked equations are solved by the SIMPLE algorithm and the set of algebraic equations are solved sequentially with the line-by-line method, which is a combination of the Gauss-Seidel method and the tridiagonal-matrix algorithm. The convergence criterion is determined by the requirement that the maximum value of the normalized residuals of any equation must be less than 1×10^{-5}.

Specifications of the dispersed phase are determined by integrating the lagrangian equations of the liquid phase in determined time steps. In each step, locations and velocities of droplets are found and mass and energy transfer between the two phases is calculated. These calculations are carried out for the fuel droplets' diameter in the range of 30 and 100 μm. The fuel spray cone angle is 60º, and the initial fuel temperature is 40ºC.

5. RESULTS

Temperature is one of the most sensitive variables in determining reaction rates and heat transfer inside the combustors. Figure 2 shows the measured and predicted radial variation of gas temperature in four axial sections: 300, 900, 1500, and 2100 mm from the furnace nozzle. It can be seen that at x=300 mm, the maximum temperature occurs in r=100 mm, where the concentration of injected fuel from 60º nozzle is at its highest level. The comparison between the measured and computed temperature levels shows that they are in good qualitative agreement, but the computed temperatures are lower than those of experimental measurements. The underpredicted results of computations can be attributed to the utilization of both the simplified two-step combustion model and the limiting capability of the four flux radiation model. The discrepancy can also be attributed to the fundamental assumption made in the combustion model used [20], which relates the rate of combustion with turbulent energy and dissipation.

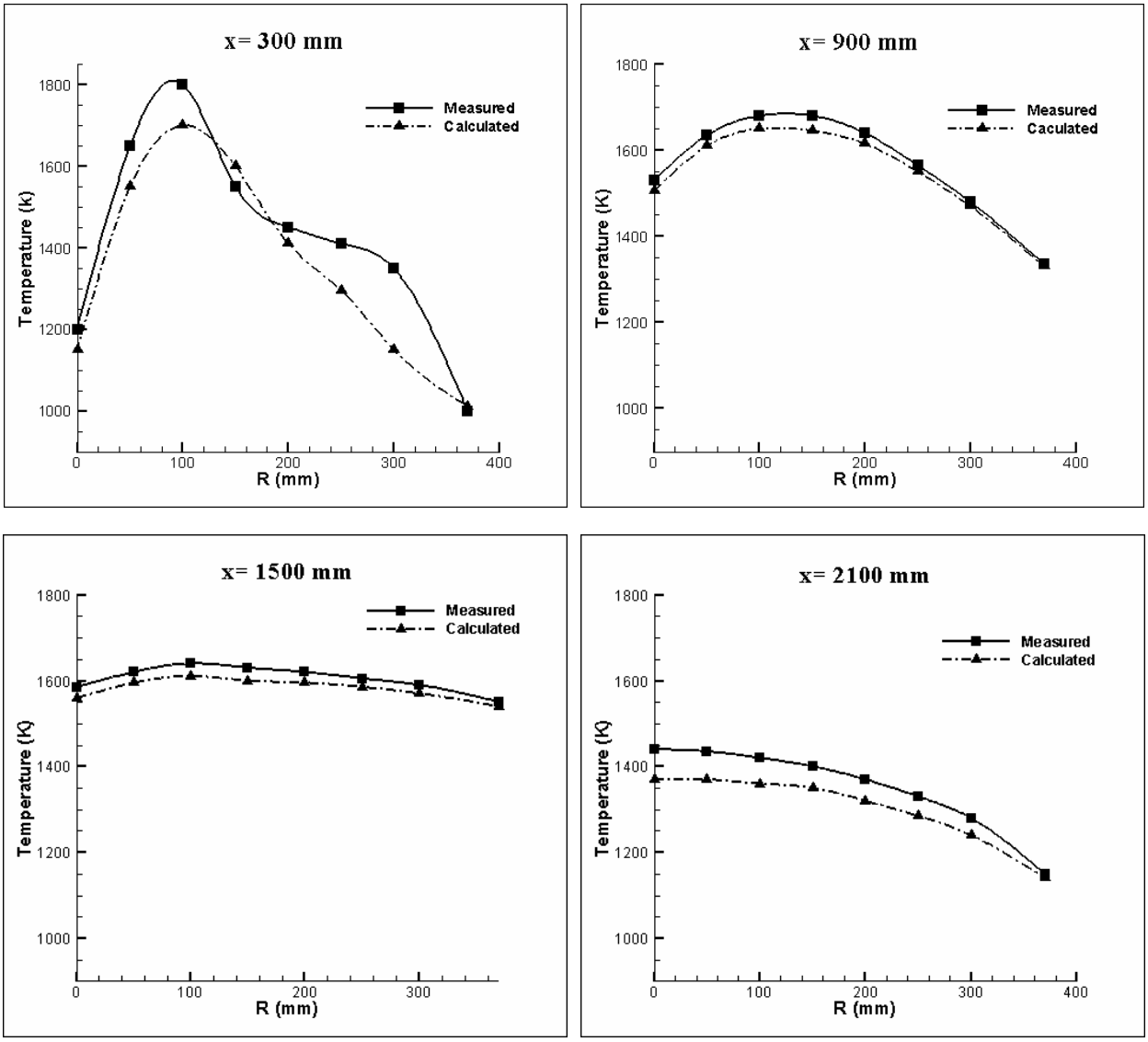

Figure 2. Radial variation of temperature in four axial sections of the furnace

It is clear that using combustion models with more steps, and considering intermediate species, can establish more accurate results. Also, a further modified radiation model is needed to account for the exchange of radiation between gas and soot particles.

Figure 3 compares the predictions of radial CO mass fraction variations in four axial sections against experimental measurements inside the combustor. CO was considered because it is one of the primary species oxidized by OH and has an affect on soot production. It is observed that predictions of CO mass fraction agree fairly well with the experimental results. As expected, the peak in the CO mass fraction occurs near the furnace inlet and r $\approx$ 100 mm. This occurs because most of the fuel evaporates near the nozzle and only after all fuel carbon is converted to CO does oxidation of the CO to CO_2 occur. The discrepancy between predicted and measured results is due to the two-step combustion model which, as mentioned earlier, underestimates the temperature levels inside the furnace.

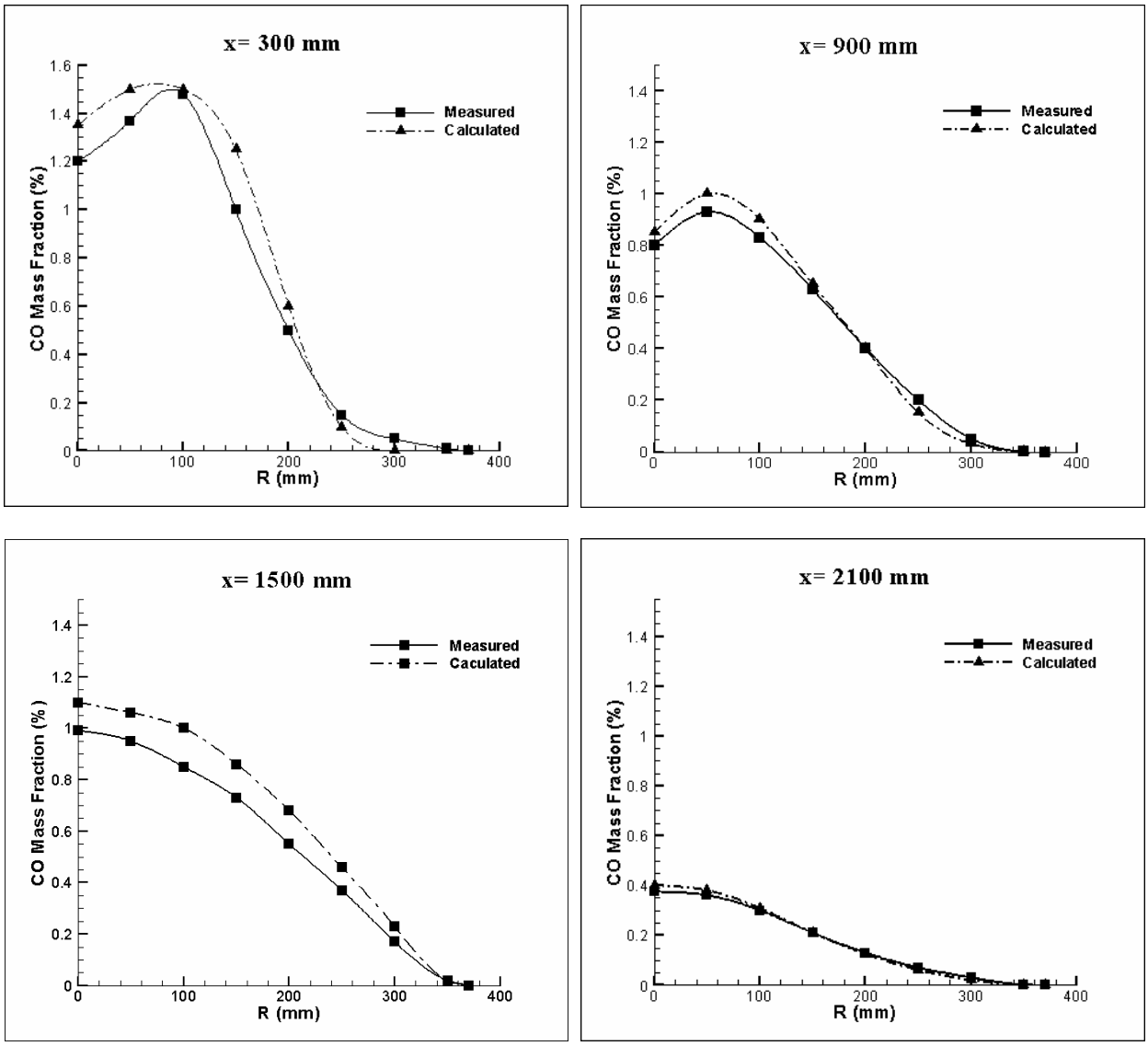

Figure 3. Radial variation of CO in four axial sections of the furnace

Figure 4 presents the measured and predicted radial variation of soot mass fraction in four axial sections. Soot precursors are pyrolized and oxidized at elevated temperatures so that maximum soot volume fraction can be seen to occur in the vicinity of the fuel injection point where the fuel concentration and temperature level are high (see Figure 2). In spray flames, the important parameters which have a profound effect on soot formation are fuel concentration and temperature [21]. The comparison between the measured and computed soot mass fractions shows good agreement. The most deviation from measured values is seen to be around the centerline, which may be due to the use of empirical factors in the mathematical soot formation model and lower levels of temperature predicted by the model (Figure 2). As mentioned above, the temperature plays an important role in the process of soot formation and it is clear from the soot model that the lower levels of temperature lead to lower values of soot concentration.

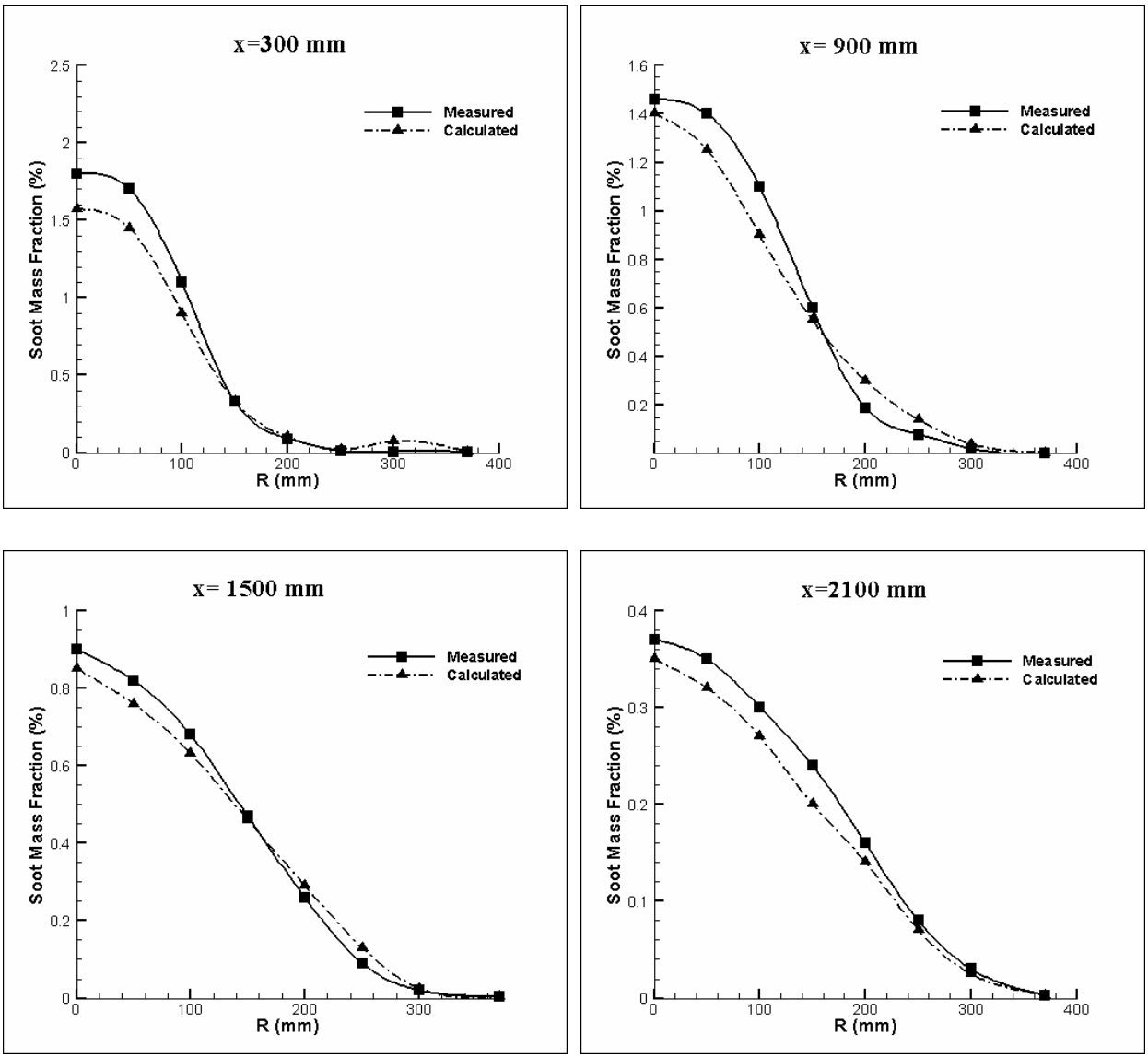

Figure 4. Radial variation of soot in four axial sections of the furnace

Figures 5 and 6 depict the effect of furnace length on predicted and measured centerline soot and CO mass fractions. It is observed that as the furnace length increases, CO and soot mass fractions decrease. This reduction of CO and soot mass fractions can be attributed to having more time for oxidation and complete combustion along the furnace. The O_2-OH oxidation model used in this study includes oxidation of soot and CO as a result of an attack by both molecular oxygen O_2 and OH radicals. As oxygen is consumed rapidly in the vicinity of the inlet port, the OH-radical is an important oxidant along the combustor. CO and soot are not oxidized until most of the fuel is consumed owing to the rapidity with which OH reacts with the fuel compared to its reaction to CO and soot [18]. It can be easily concluded by studying these figures that the length of the furnace has a remarkable impact on soot and CO emissions. Comparing the measured and calculated values reveals reasonable qualitative agreement.

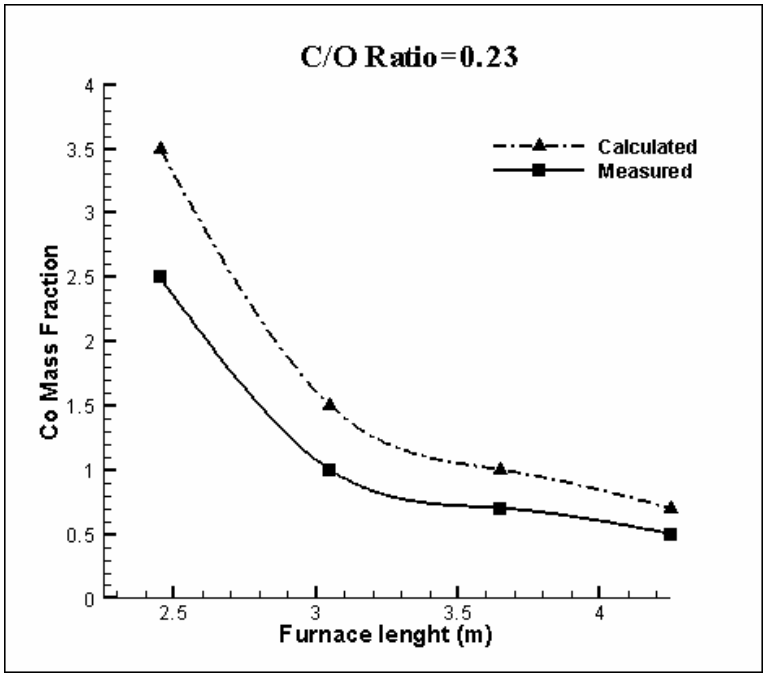

Figure 5. Effect of furnace length on CO mass fraction

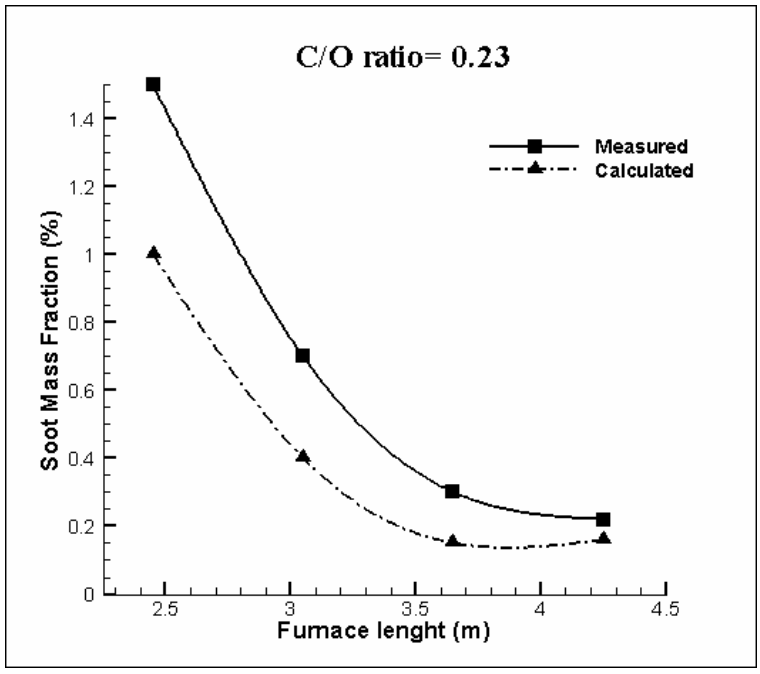

Figure 6. Effect of the furnace length on soot mass fraction

According to the reasonable agreement between the above calculated and measured results, the employed model is used to study the effect of inlet C/O ratio on the production of soot and CO in the furnace. Figure 7 presents the centerline variation of CO mass fraction for different values of inlet C/O ratio. It can be seen that the CO mass fraction increases to a maximum near the furnace inlet and then decreases. This occurs because hydrocarbon oxidation to CO is much faster than CO oxidation to CO_2. At far axial distances, the CO mass fractions are relatively unchanged, which indicates the O_2 is utilized entirely for hydrocarbon oxidation and CO oxidation is essentially frozen. The figure shows that net CO levels increase with C/O ratio.

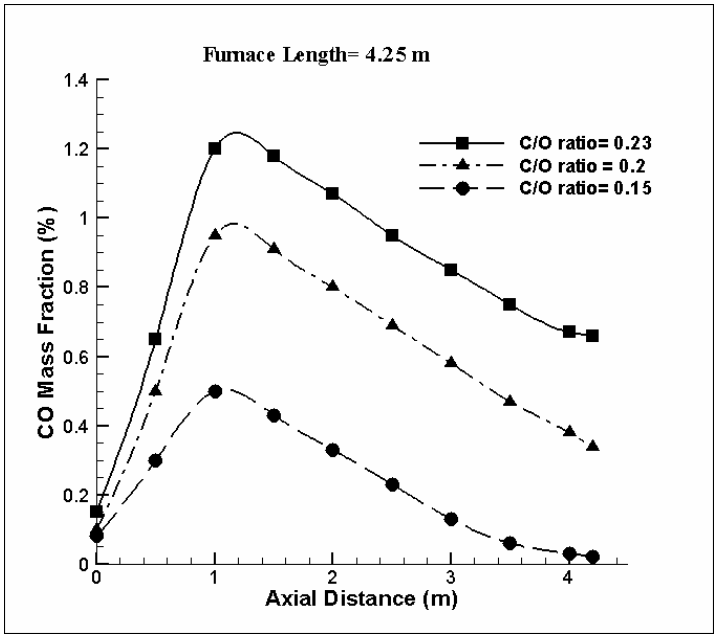

Figure 7. Effect of C/O ratio on the variation of CO mass fraction along the furnace centerline

Figure 8 shows the effect of the C/O ratio on the variation of soot mass fraction along the furnace centerline. It can be seen in a dramatic augmentation in the soot mass fraction with increasing C/O ratio. The mass fraction rises due to the initial soot formation under conditions of low O_2 and high unburned hydrocarbon. It can be seen that the centerline soot distribution increases to a maximum near the furnace inlet and then decreases. The soot particles that are initially formed either oxidize in the flame or react further to form smoke. At axial distances longer than 3200 mm, the soot mass fractions are approximately constant. The comparison between the centerline variations of CO and soot mass fractions in Figures 7 and 8 shows that the location of the maximum soot centerline coincides with the maximum CO location for different C/O ratios. A similar result was obtained for correlation between CO and soot generation factors (defined as the mass of CO or soot emitted per unit mass of fuel carbon burned) during experimental study of sooting liquid-fueled buoyant turbulent diffusion flames burning in still air [25,26]. The results show a strong correlation between mechanisms producing CO and soot in sooting flames. The results for nonsooting fuels and for the relatively lightly sooting isopropanol show that there is also a mechanism for emission of CO from turbulent diffusion flames that is not associated with soot [27].

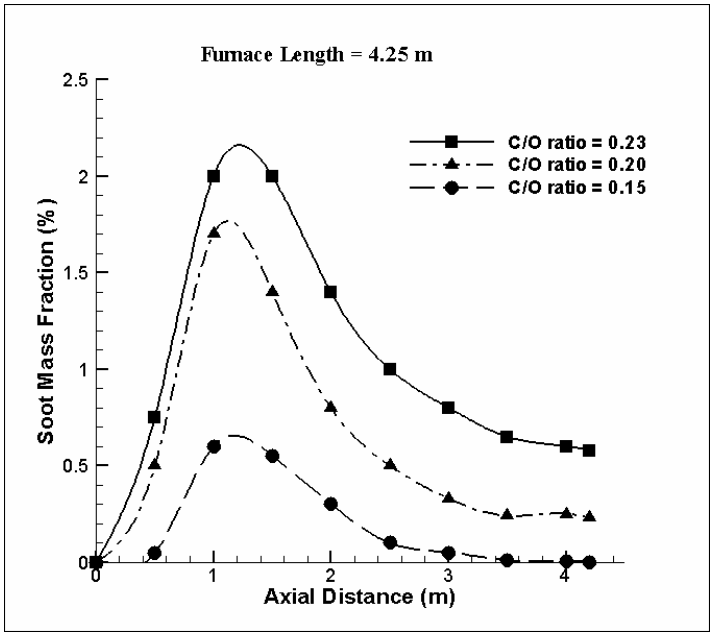

Figure 8. Effect of the C/O ratio on the variation of soot mass fraction along the furnace centerline

6. CONCLUSION

In this study, experimental measurements and numerical simulation of soot formation/combustion and CO production/emission in a large oil-fired furnace with a maximum power of 2 MW are studied. Soot and CO mass fractions inside the combustor are measured by filter paper technique and infrared analysis. A two-step process is used for combustion modeling and CO mass fraction predictions. Soot inception and surface growth are modeled through acetylene concentration. The O_2-OH oxidation model is used for investigating soot oxidation. The following conclusions are reached from the analysis of the results:

- For the stoichiometric burning condition in the vicinity of the burner inlet, due to increasing unburned hydrocarbon concentration and high temperature, a peak in the soot and CO mass fractions occurs.
- The location of soot maximum centerline profile coincides with the maximum CO location.
- An increase in the length of the furnace decreases both CO and soot mass fraction emissions
- CO and soot mass fraction emissions increase with increasing inlet C/O ratio.
- Comparison of experimental measurements with computed results shows good agreement.

REFERENCES

[1] A. Abbasi and Kh. Khoshmanesh, "Numerical Simulation and Experimental Analysis of an Industrial Glass Melting Furnace", *Applied Thermal Engineering*, **28**(2008), pp. 450–459.

[2] L. Wang, D. C. Haworth, S. R. Turns, and M. F. Modest, "Interactions Among Soot, Thermal Radiation, and NOx Emissions in Oxygen-Enriched Turbulent Non-Premixed Flames: A Computational Fluid Dynamics Modeling Study", *Combustion and Flame*, **141**(2005), pp. 170–179.

[3] N. Y. Sharma and S. K. Dom, "Influence of Fuel Volatility and Spray Parameters on Combustion Characteristics and NOx Emission in a Gas Turbine Combustor", *Applied Thermal Engineering*, **24**(2004), pp. 885–903.

[4] B. Yang and U.O. Koylu, "Detailed Soot Field in a Turbulent Non-Premixed Ethylene/Air Flame from Laser Scattering and Extinction Experiments", *Combustion and Flame*, **141**(2005), pp. 55–65.

[5] J. F. Roesler, S. Martinot, C. S. McEnally, L. D. Pfefferle, J. L. Delfau, and C. Vovelle, "Investigating the Role of Methane on the Growth of Aromatic Hydrocarbons and Soot in Fundamental Combustion Processes", *Combustion and Flame*, **134**(2003), pp.249–260.

[6] Z. A. Mansurov, "Soot Formation in Combustion Processes (Review)", *Combustion, Explosion, and Shock Waves*, **41(6)**(2005), pp. 727–744.

[7] S. J. Brookes and J. B. Moss, "Predictions of Soot Thermal Radiation Properties in Confined Turbulent Jet Diffusion Flames", *Combustion and Flame*, **116**(1999), pp. 486–503.

[8] A. Beltrame, P. Porshnev, W. Merchan-Merchan, A. Saveliev, A. Fridman, L. A. Kennedy, O. Petrova, S. Zhdanok, F. Amouri, and O. Charon, "Soot and NO Formation in Methane-Oxygen Enriched Diffusion Flames", *Combustion and Flame*, **124**(2001), pp. 295–310.

[9] M. Ilbas, N. Syred, and P. Bowen, "Experimental and Numerical Studies of a Large Oil Fired Furnace", *44th AIAA Aerospace Sciences Meeting and Exhibit*, *Reno, Nevada,* 2006.

[10] *Smoke Measurement, AVL LIST GMBH,* AVL, Graz, 2001.

[11] A. E. German and T. Mahmud, "Modelling of Non-Premixed Swirl Burner Flows Using a Reynolds-Stress Turbulence Closure", *Fuel*, **84**(2005), pp. 583–594.

[12] J. Zhang, S. Nieh, and L. Zhou, "A New Version of Algebraic Stress Model for Simulating Strongly Swirling Flows", *Numerical Heat Transfer*, **22**(1992), pp.49–62.

[13] G. H. Yeoh, R. K. K. Yuen, S. C. P. Chueng, W. K. Kwok, "On Modelling Combustion, Radiation and Soot Processes in Compartment Fires ", *Building and Environment*, **38**(2003), pp.771–785.

[14] I. Zahmatkesh and M. Moghiman, "On the Suitability of Soot Formation Models in Turbulent Flames: A Comparison Study", *Emirates Journal for Engineering Research*, **11(2)**(2006), pp. 89–98.

[15] Syed Ameer Basha and K. Raja Gopal, "In-Cylinder Fluid Flow, Turbulence and Spray Models—A Review", *Renewable and Sustainable Energy Reviews*, **13**(2009), pp. 1620–1627.

[16] J. L Xia, G. Yadigaroglu, Y. S. Liu, J. Schmidli, and B. L. Smith, "Numerical and Experimental Study of Swirling Flow in a Model Combustor", *International Journal of Heat and Mass Transfer*, **41(11)**(1998), pp. 1485–1497.

[17] S. Nesic and J. Vodnik, “Kinetics of Droplet Evaporation”, *Chemical Engineering Science*, **46(2)**(1990), pp. 527–537.

[18] K. K-Y. Kuo, *Principles of Combustion*. *2nd Ed*. New York, NY: Wiley-Interscience, 2005.

[19] B. F. Magnussen and M. H. Hjertager, "On Mathematical Modeling of Turbulent Combustion, With a Special Emphasis on Soot Formation and Combustion", *16th Symp. (Int.), on Combustion, the Combustion Institute*, (1977), pp. 716–729.

[20] J. B. Moss, C. D. Stewart, and K. J. Young, "Modeling Soot Formation and Oxidation in a High Temperature Laminar Diffusion Flame Burning Under Oxygen-Enriched Conditions", *Combustion and Flame*, **101**(1995), pp. 491–500.

[21] K. Bashirnezhad, M. Moghiman, and I. Zahmatkesh, "An Investigation of Soot Formation and Combustion in Turbulent Spray Flames", *Kuwait J. Sci. Eng*. **34(1B)**(2007), pp.183–202.

[22] Z. Wen, S. Yun, M. J. Thomson, and M. F. Lightstone, "Modeling Soot Formation in Turbulent Kerosene/Air Jet Diffusion Flames", *Combustion and Flame*, **135**(2003), pp. 323–340.

[23] N. Syred, K. Kurniawan, T. Griffiths, T. Gralton, and R. Ray, "Development of Fragmentation Models for Solid Fuel Combustion and Gasification as Subroutines for Inclusion in CFD Codes", *Fuel*, **86(14)**(2007), pp. 2221–2231.

[24] J. H. Ferziger and M. Peric, *Computational Methods for Fluid Dynamics*, *Third Rev. Edition,* Springer, 2002.

[25] Y. R. Sivathanu and G. M. Faeth, “Soot Volume Fractions in the Overfire Region of Turbulent Diffusion Flames”, *Combust. Flame*, **81**(1990), pp. 133–149.

[26] U. O. Koyulu, Y. R. Sivathanu, and G. M. Faeth, "Carbon Monoxide and Soot Emissions from Buoyant Turbulent Diffusion Flames", *Fire Safety Science*, *Proceedings of the Third International Symposium, (G. Cox and B. Langford eds.)* London: Elsevier Science Publishers Ltd., 1991.

[27] U. O. Koyulu and G. M. Faeth, “Carbon Monoxide and Soot Emissions from Liquid-Fueled Buoyant Turbulent Diffusion Flames”, *Combust. Flame*, **87**(1991), pp. 61–76.